

# Sequential Integrity Monitoring for Kalman Filter Innovations-Based Detectors

Çağatay Tanil, Samer Khanafseh, *Illinois Institute of Technology*,  
Mathieu Joerger, *The University of Arizona*,  
Boris Pervan, *Illinois Institute of Technology*

## BIOGRAPHIES

**Dr. Çağatay Tanil** received his B.S. and M.S. in Mechanical Engineering from Middle East Technical University, in 2006 and 2009, respectively; and Ph.D. in Aerospace Engineering from Illinois Institute of Technology (IIT) in 2016. His doctoral work, detecting GNSS spoofing attacks using INS coupling, won the 2017 Institute of Navigation (ION) Bradford W. Parkinson Award for excellence in global navigation satellite systems. With more than 12 years of guidance, navigation, and control experience, Dr. Tanil fulfilled many research and development roles such as dynamic modeling and simulation, guidance and control of missiles. From 2006-2013, he worked at leading defense and aerospace companies in Turkey, including Roketsan Missiles Industries, Turkish Aerospace Industries (TAI), and Defense Industries Research and Development Institute (Tubitak-SAGE). Dr. Tanil is currently a Senior Research Associate at IIT and a Research Scientist at TruNav LLC, working on sensor fusion (INS/GNSS) and estimation, fault/spoofing detection, and integrity monitoring for high precision navigation and guidance systems.

**Dr. Samer Khanafseh** is currently a research assistant professor at Illinois Institute of Technology (IIT), Chicago. He received his MSc and PhD degrees in Aerospace Engineering from IIT in 2003 and 2008, respectively. Dr. Khanafseh has been involved in several aviation applications such as Autonomous Airborne Refueling (AAR) of unmanned air vehicles, autonomous shipboard landing for NUCAS and JPALS programs and Ground Based Augmentation System (GBAS). His research interests are focused on high accuracy and high integrity navigation algorithms, cycle ambiguity resolution, high integrity applications, fault monitoring and robust estimation techniques. He was the recipient of the 2011 Institute of Navigation Early Achievement Award for his outstanding contributions to the integrity of carrier phase navigation systems.

**Dr. Mathieu Joerger** obtained a Diplome d'Ingenieur in Mechatronics from the National Institute of Applied Sciences in Strasbourg, France, in 2002, and a M.S. and a Ph.D. in Mechanical and Aerospace Engineering from the Illinois Institute of Technology (IIT), in 2002 and 2009 respectively. He is the 2009 recipient of the Institute of Navigation (ION) Parkinson award, and the 2014 recipient of the IONs Early Achievement Award. He is currently an assistant professor at The University of Arizona, working on multi-sensor integration, sequential fault-detection for multi-constellation navigation systems, and relative and differential receiver autonomous integrity monitoring (RAIM).

**Dr. Boris Pervan** is a Professor of Mechanical and Aerospace Engineering at IIT, where he conducts research on advanced navigation systems. Prior to joining the faculty at IIT, he was a spacecraft mission analyst at Hughes Aircraft Company (now Boeing) and a postdoctoral research associate at Stanford University. Prof. Pervan received his B.S. from the University of Notre Dame, M.S. from the California Institute of Technology, and Ph.D. from Stanford University. He is an Associate Fellow of the AIAA, a Fellow of the Institute of Navigation (ION), and Editor-in-Chief of the ION journal NAVIGATION. He was the recipient of the IIT Sigma Xi Excellence in University Research Award (2011, 2002), Ralph Barnett Mechanical and Aerospace Dept. Outstanding Teaching Award (2009, 2002), Mechanical and Aerospace Dept. Excellence in Research Award (2007), University Excellence in Teaching Award (2005), IEEE Aerospace and Electronic Systems Society M. Barry Carlton Award (1999), RTCA William E. Jackson Award (1996), Guggenheim Fellowship (Caltech 1987), and Albert J. Zahm Prize in Aeronautics (Notre Dame 1986).

## ABSTRACT

This paper describes the derivation, analysis and evaluation of a new sequential integrity monitoring for Kalman filter (KF) applications. The monitor uses innovation sequence obtained from a single Kalman filter for fault detection. Unlike multiple hypothesis solution separation monitors, it does not require running sub-filters to detect and exclude the fault. The main contributions of this paper is an analytical recursive expression of the worst case failure mode slopes, which is direct means of computing protection levels in real-time. The performance of the monitor is evaluated and verified against single satellite faults through a tightly-coupled INS/GNSS integrated navigation systems in aircraft approach and en route operations. However, the methodology developed in this paper is not limited to INS/GNSS systems but applicable to any other multi-sensor systems using KF estimators.

## I. INTRODUCTION

Of primary concern in safety critical applications is integrity, which is a measure of trust in sensor information. The integrity risk is defined as the probability of a system state estimation error exceeding a predefined limit of acceptability (or alert limit) without timely warnings. For example, in aircraft final approach applications, states of interest include the aircraft's vertical position coordinate, and, the alert limit ranges from ten to tens of meters depending on the mission. For ground transportation applications, especially self-driving cars, the lateral alert limits are in sub-meter levels. Therefore, alert mechanisms are required to guarantee the positioning integrity. The challenge in integrity monitoring is not so much to design estimators and detectors, as it is to quantify the risk of undetected faults causing estimation errors to exceed the alert limit. Because sensor faults are rarely occurring events, we know very little about them other than, sometimes, their mean rate of occurrence. To address this problem, and to account for the impact of undetected faults on estimation errors, worst-case approaches are adopted.

In this work, we assume that faults cause unknown, time-varying shifts in mean measurement error. On the one hand, large-size faults have a significant impact on estimation error but are easy to detect. On the other hand, smaller and slow building faults will likely go undetected, but will not impact estimation error much. Thus, integrity monitoring can be seen as an optimization process: finding the worst-case fault, which maximizes estimation error while going undetected, thereby maximizing integrity risk. For snapshot estimators and detectors, analytical solutions exist to find the worst-case fault vector magnitude and direction, even when multiple measurements are simultaneously faulted [8], [4]. If robust time-propagation models for state estimate and measurement errors are available, then time-sequential estimators, such as a KF, surpass snapshot estimators in accuracy performance. Under the same assumptions, sequential detectors can be significantly more efficient than snapshot detectors, especially against slowly increasing faults.

Multiple-Hypothesis Solution Separation (MHSS) can be used for integrity monitoring in time-sequential implementations [7]. In MHSS, under a given fault hypothesis, the detection test statistic is the difference between the full-set solution and the subset fault-free solution that excludes all faulty observations. The main drawback of MHSS is that it requires banks of KFs for each fault hypothesis, which brings a heavy computational burden especially in the existence of multiple sensor faults and a higher risk of false alarms due to multiple tests [4], [9]. In contrast, a chi-squared detector uses a single test statistic. We can distinguish two chi-squared test statistics, either derived from the weighted norm of KF measurement residuals, or innovations. In this work, we focus on the latter because its distribution is easier than that of residuals in quantifying the integrity risk. The innovation-based test statistic, which is the sum of weighted norms squared for a sequence of KF innovations is chi-squared distributed [1].

A major challenge with a KF estimator and an innovation-based (IB) detector is to find the worst-case fault profile over time that maximizes integrity risk. A first answer to this question was provided in [1]. It showed that, in general, the worst-case fault profile is neither a step, a ramp, nor a quadratic function, which are often assumed when no other methods were available. The mathematical framework to quantify integrity risk described in [1] captures the impact of fault history on estimation error and innovations using block matrices obtained from time propagation of KF. These block matrices were used to determine the maximum failure-mode slope (FMS), the maximum ratio of the mean estimation error over the non-centrality parameter of the test statistic. Unfortunately, this approach is computationally limited due to growing size block matrices, especially for en route aircraft operations requiring a

larger fault monitoring window. In response, this work describes a fully recursive approach to compute the worst-case fault, thereby providing a rigorous and computationally efficient method to upper-bound the integrity risk in widely-used KF applications.

This paper describes a new sequential integrity monitoring for Kalman filter (KF) applications. Its integrity and computational performance are superior to the existing baseline A-RAIM (Advanced Receiver Autonomous Integrity Monitoring) techniques using solution-separation-based monitors. There are mainly two reasons for that: 1) Unlike snapshot A-RAIM techniques, the proposed monitor utilizes a time sequence of a single KF innovations for fault detection that leverages satellite motion over time, especially against gradual and consistent constellation faults, 2) It incorporates onboard inertial sensors without any modification to the receivers, which tremendously increases the monitor's immunity to faults in the existence of poor satellite visibility or signal spoofing where all the baseline A-RAIM techniques lose their functions.

In the first part of the paper, we present a derivation for a sequential update of the worst-case FMS. For time sequential monitors, detecting gradual faults is much more difficult than that on abrupt faults, therefore the resulting worst-case FMS may increase as the time window for fault gets longer [1]. On the other hand, when only a sub-set of measurements are faulty the maximum FMS may be bounded over time since the redundancy due to the healthy measurement will increase as time elapses, which offers more opportunities to detect a fault, especially when using accumulated innovation norm. The key step in the derivation is capturing the impact of the fault time and the unfaulty measurements on the worst-case FMS in a sequential formulation, which is composed of a successive time update and fault downdate processes. The FMS time update equation is obtained by simplifying the block matrix approach previously developed in [1], by using matrix inversion lemmas. The fault downdate equation is obtained using rank one update methods [2]. It is remarkable that the worst-case FMS recursion is established on a square matrix with a dimension of the number of KF states and does not require any inversion. This is of fundamental importance implying that lower computation and memory resources are required to provide a tight integrity risk bound.

Innovations sequence monitors when used with a single Kalman filter, does not have the capability of excluding faulty measurements. It is common to use bank of sub-filters with solution separation methods to bring the exclusion capability, which however comes with the computational cost of multiple filters. By means of the sequential FMS approach, the second part of the paper constructs a mathematical framework for fault exclusion without needing to run multiple filters.

In the final section of the paper, we evaluate the innovation sequence monitor on an integrated INS/GNSS navigation systems. Using the sequential approach worst-case FMS values, resulting integrity risks are recorded and verified against those obtained from the block matrix approach developed in the prior work. The leverage of satellite motion and inertial sensors are quantified. For aircraft approach and en route aircraft operations, it is demonstrated that the proposed monitor meets all RNP0.1, RNP0.3, LPV200, CAT-I, and CAT-II/III integrity requirements in the existence of minimal satellite redundancy (e.g. minimum 5 or more satellites in view). In the absence of satellite redundancy where all baseline A-RAIM monitors fail, it was shown that the proposed INS monitor still guarantees LPV200 and CAT-I integrity while it preserves integrity for limited (but reasonable) durations for the CAT-II/III, RNP0.1, and RNP0.3.

## II. KALMAN FILTER INNOVATION SEQUENCE MONITOR

Kalman filter innovation monitoring is a common feature of Kalman filter applications. It is useful for detecting short-term faults. When monitoring snapshot innovations, the monitor responds poorly to faults that build up gradually. The reason is that the state estimates are corrupted before the fault becomes hazardous. However, slowly growing faults can be identified by forming a test statistic containing the past and current innovations. This is known as innovation sequence monitoring [10].

Let process and measurement models be

$$\mathbf{x}_k = \Phi_k \mathbf{x}_{k-1} + \Gamma_{k-1} \tilde{\mathbf{u}}_{k-1} + \mathbf{w}_k \quad (1)$$

$$\mathbf{z}_k = \mathbf{H}_k \mathbf{x}_k + \nu_k \quad (2)$$

where  $\Phi$  ( $m \times m$ ) is the state transition matrix of the process model,  $\tilde{\mathbf{u}}_k$  ( $1 \times 1$ ) is deterministic input to the process,  $\Gamma$  ( $m \times 1$ ) is the input coefficient matrix,  $\mathbf{w}_k \sim \mathcal{N}(0, \mathbf{W}_k)$  ( $m \times 1$ ) is the process noise,  $\mathbf{H}_k$  ( $n \times m$ ) is the observation matrix, and  $\nu_k \sim \mathcal{N}(0, \mathbf{V}_k)$  is the measurement noise vector ( $n \times 1$ ).

Then, the Kalman filter time update can be written as

$$\bar{\mathbf{x}}_k = \Phi_{k-1} \hat{\mathbf{x}}_{k-1} + \Gamma_{k-1} \tilde{\mathbf{u}}_{k-1} \quad (3)$$

where  $\bar{\mathbf{x}}_k$  is the a priori estimate of  $\mathbf{x}_k$ .

And, the measurement update gives the a posteriori estimate  $\hat{\mathbf{x}}_k$  as

$$\hat{\mathbf{x}}_k = \bar{\mathbf{x}}_k + \mathbf{L}_k (\mathbf{z}_k - \mathbf{H}_k \bar{\mathbf{x}}_k) \quad (4)$$

where  $\mathbf{L}_k$  ( $m \times n$ ) is the optimal Kalman gain.

Based on the Kalman filter estimator defined in (3) and (4), one can define a detector that utilizes the Kalman filter innovation sequence as follows:

Let an innovation vector  $\gamma_k$  be

$$\gamma_k = \mathbf{z}_k - \mathbf{H}_k \bar{\mathbf{x}}_k, \quad (5)$$

then a test statistic  $q_k$  can be defined as the sum of squares of the normalized innovation sequence as

$$q_k = \sum_{i=1}^k \gamma_i^T \mathbf{S}_i^{-1} \gamma_i \quad (6)$$

where  $\mathbf{S}_i$  is innovation vector covariance matrix at epoch  $i$ .

The innovation sequence monitor simply checks whether the test statistic  $q_k$  is smaller than a pre-defined threshold  $T_k^2$  as

$$q_k \geq T_k^2 \quad (7)$$

Under fault free conditions, the test statistic  $q_k$  at the  $k^{\text{th}}$  measurement update is chi-square distributed with  $kn$  degrees of freedom. For a given false alarm requirement, the threshold  $T_k^2$  is determined from the inverse chi-square innovation sequence distribution function. The monitor alarms for a fault if  $q_k > T_k^2$ . Under faulted conditions,  $q_k$  is non-centrally chi-square distributed with a non-centrality parameter  $\lambda_k^2$ ,

$$\lambda_k^2 = \sum_{i=1}^k \mathbb{E}[\gamma_i^T] \mathbf{S}_i^{-1} \mathbb{E}[\gamma_i] \quad (8)$$

which is used to evaluate the probability of missed detection. It should be noted that selection of the innovation sample size is a trade off between detector's response time and sensitivity to slow faults, that is the longer the sample size, the less sensitive the monitor is whereas it has a faster response time faults as the sample size gets smaller.

### III. INTEGRITY RISK AND FAILURE MODE SLOPE FOR PERFORMANCE EVALUATION

Under fault hypothesis, the measurement vector  $\mathbf{z}_k$  in (4) and (5) can be replaced by  $\mathbf{z}_k + \mathbf{f}_k$  where  $\mathbf{f}_k$  is a ( $n \times 1$ ) fault vector that contains fault for each measurement. In this work, integrity risk, the probability that the state estimate error exceeds an alert limit without being detected (i.e.,  $q < T^2$ ), is used as a metric to quantify the performance of the innovation sequence monitor. Assuming a prior fault probability of  $P_{H_i}$ , for a given  $\mathbf{f}_k$  the integrity risk associated with  $i^{\text{th}}$  hypothesis is expressed in terms of the test statistic  $q_k$  and the estimate error  $\varepsilon_k$  as

$$I_{r_k} = P(|\varepsilon_k| > \ell, q_k < T_k^2 | \mathbf{f}_k) P_{H_i} \quad (9)$$

where  $\ell$  is the vertical alert limit, and  $T_k^2$  is pre-defined threshold for detection. The error associated with the state of interest,  $\varepsilon_k$ , can be extracted from the state estimate error vector  $\tilde{\mathbf{x}}_k = \hat{\mathbf{x}}_k - \mathbf{x}_k$  using the row transformation vector  $\mathbf{T}_\varepsilon$  as  $\varepsilon_k = \mathbf{T}_\varepsilon \tilde{\mathbf{x}}_k$ . Since  $\mathbb{E}[\tilde{\mathbf{x}}_i \gamma_j^T] = 0$ , which was shown in [1], the test statistic  $q_k$  obtained from  $\gamma_1 \dots \gamma_k$ ,

and the error state of interest  $\varepsilon_k$  obtained from  $\tilde{\mathbf{x}}_k$ , will be statistically independent. As a result, the integrity risk  $I_{r_k}$  can be written as a product of two probabilities

$$I_{r_k} = P(|\varepsilon_k| > \ell \mid \mathbf{f}_k) P(q_k < T_k^2 \mid \mathbf{f}_k) P_{H_i} \quad (10)$$

In order to protect the system against all potential faults, the integrity risk must be conservatively evaluated. An upper bound on the integrity risk can be determined by computing a worst-case failure mode (FMS),  $\rho_k^2 = \mathbb{E}[\varepsilon_k]^2 / \lambda_k^2$ , that is maximizing the position estimate error (most hazardous) while minimizing the non-centrality of the chi-square test statistic (most misleading):

$$\arg \max_{\tilde{\mathbf{x}}_k} \rho_k^2 = \frac{\mathbb{E}[\tilde{\mathbf{x}}_k^T] \mathbf{t}_\varepsilon^T \mathbf{t}_\varepsilon \mathbb{E}[\tilde{\mathbf{x}}_k]}{\lambda_k^2}. \quad (11)$$

The worst-case failure mode slope(FMS)  $\rho_k^{*2}$  for Kalman filter estimators, was previously derived in [1] using a block matrix approach. However, this approach is computationally expensive because it uses block matrices that are growing unboundedly over time. This paper addresses this problem by developing a recursive approach to obtain FMS.

#### IV. A REVIEW OF BLOCK MATRIX SOLUTION TO FAILURE MODE SLOPE

This section is a review the block matrix approach which will be a foundation to recursive approach in the next section.

Replacing  $\mathbf{z} = \mathbf{z} + \mathbf{f}$  and  $\hat{\mathbf{x}} = \mathbf{x} + \tilde{\mathbf{x}}$  in Kalman filter equations through (1)-(4), one can derive a sequential form of the means of state estimate error  $\tilde{\mathbf{x}}_k$  ( $m \times 1$ ) and innovation  $\gamma_k$  ( $n \times 1$ ) in terms of  $\mathbf{f}$  as [1]:

$$\mathbb{E}[\tilde{\mathbf{x}}_k] = (\mathbf{I} - \mathbf{L}_k \mathbf{H}_k) \Phi_k \mathbb{E}[\tilde{\mathbf{x}}_{k-1}] + \mathbf{L}_k \mathbf{f}_k \quad (12)$$

$$\mathbb{E}[\gamma_k] = -\mathbf{H}_k \Phi_k \mathbb{E}[\tilde{\mathbf{x}}_{k-1}] + \mathbf{f}_k. \quad (13)$$

To generalize (12) and (13) for subset measurement faults, in which case  $\mathbf{f}_k$  will have zero rows, one can decompose  $\mathbf{f}_k$  as

$$\mathbf{f}_k = \mathbf{T}_k \bar{\mathbf{f}}_k \quad (14)$$

where  $\bar{\mathbf{f}}_k$  ( $r \times 1$ ) is a non-zero fault vector,  $\mathbf{T}_k$  ( $n \times r$ ) is an orthogonal transformation matrix It simply adds zeros to corresponding fault-free measurement rows,  $r$  is the number of faulty measurements and  $1 < r \leq n$ . It should be noted that Note that  $\mathbf{T}_k^T \mathbf{T}_k = \mathbf{I}$  and for full-set measurement fault case it can be simplified as  $\mathbf{T}_k = \mathbf{I}$ .

Given a fault-free initial condition as  $\mathbb{E}[\tilde{\mathbf{x}}_0] = \mathbb{E}[\gamma_0] = \mathbf{0}$ , the particular solution to the difference equation (12) is obtained as a function of  $\bar{\mathbf{f}}_{1:k}$  as

$$\mathbb{E}[\tilde{\mathbf{x}}_k] = \underbrace{[\mathbf{A}_{1k} \mathbf{T}_1 \ \dots \ \mathbf{A}_{kk} \mathbf{T}_k]}_{\mathbf{A}_{1:k}} \underbrace{\begin{bmatrix} \mathbf{f}_1 \\ \vdots \\ \mathbf{f}_k \end{bmatrix}}_{\bar{\mathbf{f}}_{1:k}} \quad (15)$$

where

$$\mathbf{A}_{ij} = \begin{cases} \left( \prod_{t=j}^{i+1} (\mathbf{I} - \mathbf{L}_t \mathbf{H}_t) \Phi_t \right) \mathbf{L}_i & \text{if } i < j \\ \mathbf{L}_i & \text{if } i = j \end{cases} \quad (16)$$

where  $\mathbf{A}_{1:k}$  ( $m \times rk$ ) is a horizontally growing size matrix containing current and past Kalman filter information whereas  $\mathbf{A}_{ik}$  ( $m \times n$ ) has a constant size containing only the current time information.

Substituting (15) into (13) gives the mean of innovation as a function of  $\bar{\mathbf{f}}_{1:k}$  as

$$\mathbb{E}[\gamma_k] = \underbrace{[-\mathbf{H}_k \Phi_k \mathbf{A}_{1:k-1} \ \mathbf{T}_k]}_{\mathbf{B}_k} \underbrace{\begin{bmatrix} \bar{\mathbf{f}}_{1:k-1} \\ \mathbf{f}_k \end{bmatrix}}_{\bar{\mathbf{f}}_{1:k}} \quad (17)$$

where  $\mathbf{B}_k$  ( $n \times rk$ ) is also horizontally growing matrix.

Using (6), the non-centrality of the test statistic can be written as

$$\lambda_k^2 = \sum_{i=1}^k \bar{\mathbf{f}}_{1:i}^\top \mathbf{B}_i^\top \mathbf{S}_i^{-1} \mathbf{B}_i \bar{\mathbf{f}}_{1:i}. \quad (18)$$

Let  $\bar{\mathbf{B}}_i = [\mathbf{B}_i \quad \mathbf{0}_{n \times r(k-i)}]$  and  $0 < i < k$ . Then, (18) is equivalently expressed in block matrix form as

$$\lambda_k^2 = \bar{\mathbf{f}}_{1:k}^\top \underbrace{[\bar{\mathbf{B}}_1^\top \dots \bar{\mathbf{B}}_k^\top]}_{\mathbf{S}_{1:k}^{-1}} \underbrace{\begin{bmatrix} \mathbf{S}_1^{-1} & & \\ & \ddots & \\ & & \mathbf{S}_k^{-1} \end{bmatrix}}_{\bar{\mathbf{B}}_{1:k}} \bar{\mathbf{f}}_{1:k} \quad (19)$$

where  $\bar{\mathbf{B}}_{1:k}$  ( $nk \times rk$ ) is a lower block triangular matrix that grows both horizontally and vertically over time. Note that for full-set measurement fault, that is  $r = n$ , it will be a square matrix, therefore invertible; otherwise it will be rectangular matrix.

Substituting (15), (19) into (11) gives the FMS  $\rho_k$  as a function of the fault sequence  $\mathbf{f}_{1:k}$  as

$$\rho_k^2 = \frac{\bar{\mathbf{f}}_{1:k}^\top \mathbf{A}_{1:k}^\top \mathbf{t}_\varepsilon^\top \mathbf{t}_\varepsilon \mathbf{A}_{1:k} \bar{\mathbf{f}}_{1:k}}{\bar{\mathbf{f}}_{1:k}^\top \bar{\mathbf{B}}_{1:k}^\top \mathbf{S}_{1:k}^{-1} \bar{\mathbf{B}}_{1:k} \bar{\mathbf{f}}_{1:k}}. \quad (20)$$

The direction of fault sequence vector  $\bar{\mathbf{f}}_{1:k}$  that maximizes  $\rho_k^2$  in (20), was derived in [1], and the associated worst-case (maximum) FMS was obtained in terms of growing size matrices  $\mathbf{A}_{1:k}$  and  $\bar{\mathbf{B}}_{1:k}$  as

$$\rho_k^{*2} = \mathbf{t}_\varepsilon \mathbf{A}_{1:k} (\bar{\mathbf{B}}_{1:k}^\top \mathbf{S}_{1:k}^{-1} \bar{\mathbf{B}}_{1:k})^{-1} \mathbf{A}_{1:k}^\top \mathbf{t}_\varepsilon^\top \quad (21)$$

The block matrix approach reviewed above, computationally infeasible for infinite time Kalman filter processes. However, (21) and the definition of the growing size matrices provide a foundation for developing a sequential formulation for the FMS, which is covered in the next section.

## V. SEQUENTIAL SOLUTION TO FAILURE MODE SLOPE

Recursive expressions of each of the growing size matrices,  $\bar{\mathbf{B}}_{1:k}$ ,  $\mathbf{A}_{1:k}$ ,  $\mathbf{S}_{1:k}^{-1}$ , are the first step to achieve a recursive formulation to the FMS expression in (21). These individual terms are easy to recursively express, however the inverse of parenthesis in (21) requires meticulous block matrix inversion operations. This section will describe the key steps in the recursive formulation derivations, yet leave the exhausting parts of the derivations to Appendices A and B.

Eq. (16) suggests  $\mathbf{A}_{i:k} = (\mathbf{I} - \mathbf{L}_k \mathbf{H}_k) \Phi_k \mathbf{A}_{i\{k-1\}}$  for  $i \neq k$  and  $\mathbf{A}_{k:k} = \mathbf{L}_k$ . Substituting these into the definition of  $\mathbf{A}_{1:k}$  in (15) yields:

$$\mathbf{A}_{1:k} = [(\mathbf{I} - \mathbf{L}_k \mathbf{H}_k) \Phi_k \mathbf{A}_{1:k-1} \quad \mathbf{L}_k \mathbf{T}_k] \quad (22)$$

Eq. (19) shows that  $\mathbf{S}_{1:k}$  is a block diagonal and symmetric matrix, therefore its recursive expression is trivial:

$$\mathbf{S}_{1:k}^{-1} = \begin{bmatrix} \mathbf{S}_{1:k-1}^{-1} & \mathbf{0} \\ \mathbf{0} & \mathbf{S}_k^{-1} \end{bmatrix}. \quad (23)$$

Also, using the definitions in (17) and (19),  $\bar{\mathbf{B}}_{1:k}$  can be written as

$$\bar{\mathbf{B}}_{1:k} = \begin{bmatrix} \bar{\mathbf{B}}_{1:k-1} & \mathbf{0} \\ -\mathbf{H}_k \Phi_k \mathbf{A}_{1:k-1} & \mathbf{T}_k \end{bmatrix}. \quad (24)$$

Unfortunately, the inversion term  $(\bar{\mathbf{B}}_{1:k}^\top \mathbf{S}_{1:k}^{-1} \bar{\mathbf{B}}_{1:k})^{-1}$  in (21) grows in size over time and does not have an explicit recursive expression. However, one can notice that the whole term  $\mathbf{A}_{1:k} (\bar{\mathbf{B}}_{1:k}^\top \mathbf{S}_{1:k}^{-1} \bar{\mathbf{B}}_{1:k})^{-1} \mathbf{A}_{1:k}^\top$  in (21) is an  $m \times m$

matrix of which size is bounded by the number of states in Kalman filter. Using block matrix inversion lemmas [3] its semi-recursive expression is obtained in Appendix A as

$$\mathbf{A}_{1:k}(\overline{\mathbf{B}}_{1:k}^{\top} \mathbf{S}_{1:k}^{-1} \overline{\mathbf{B}}_{1:k})^{-1} \mathbf{A}_{1:k}^{\top} = \mathbf{R}_k \mathbf{A}_{1:k-1} (\overline{\mathbf{B}}_{1:k-1}^{\top} \mathbf{S}_{1:k-1}^{-1} \overline{\mathbf{B}}_{1:k-1} + \mathbf{A}_{1:k-1}^{\top} \mathbf{J}_k \mathbf{A}_{1:k-1})^{-1} \mathbf{A}_{1:k-1}^{\top} \mathbf{R}_k^{\top} + \mathbf{K}_k \quad (25)$$

where  $\mathbf{K}_k$  and  $\mathbf{R}_k$  are full-rank ( $m \times m$ ) matrices, and  $\mathbf{J}_k$  ( $m \times m$ ) has  $(n-r)$  rank. The definition of each is given in terms of current time Kalman filter parameters (i.e.,  $\Phi_k$ ,  $\mathbf{H}_k$ ,  $\Phi_k$ ,  $\mathbf{S}_k$ ,  $\mathbf{L}_k$ , and  $\mathbf{T}_k$ ) in Appendix A.

Eq. (25) in its current form, is not fully recursive due to the second term inside the inverse parenthesis. Due to  $\mathbf{J}_k$  multiplication, the second term has also  $(n-r)$  rank and one can notice that it is the direct effect of  $(n-r)$  fault-free measurements on the worst-case FMS. That is, the FMS will get smaller as the number of healthy measurements increases in the system. If there is no fault-free measurement in the system, this term will be zero (i.e.,  $n=r$ ), then the ‘time update’ recursion of FMS will be fully sequential and complete.

For subset measurement fault hypothesis, an additional recursion, which is over fault-free satellite measurements from 1 to  $(n-r)$  at each time epoch  $k$ , is inevitable, which we later define as ‘fault downdate’.

To do that,  $(n-r)$  rank  $\mathbf{J}_k$  matrix is first defined as

$$\mathbf{J}_k = \mathbf{J}_k^{(1)} + \mathbf{J}_k^{(2)} + \dots + \mathbf{J}_k^{(n-r)} \quad (26)$$

where each  $\mathbf{J}_k^{(j)}$  has rank 1 and can be obtained by singular value decomposition of the highlighted term in  $\mathbf{J}_k$  where  $1 \leq j \leq n-r$ ; or simply zeroing all of its rows except the  $j^{\text{th}}$  row where  $1 \leq j \leq n$ . Note that the latter might be computationally less expensive.

Then let us define a matrix

$$\mathbf{N}_k^{(i)} \triangleq \begin{cases} \overline{\mathbf{B}}_{1:k}^{\top} \mathbf{S}_{1:k}^{-1} \overline{\mathbf{B}}_{1:k} + \sum_{j=1}^i \mathbf{A}_{1:k}^{\top} \mathbf{J}_{k+1}^{(j)} \mathbf{A}_{1:k} & \text{if } i > 0 \\ \overline{\mathbf{B}}_{1:k}^{\top} \mathbf{S}_{1:k}^{-1} \overline{\mathbf{B}}_{1:k} & \text{if } i = 0 \end{cases} \quad (27)$$

where using (26) each term of the summation in (27) will have rank 1. It should also be noted that  $\mathbf{N}_k^{(j)}$  is rank-1 update of  $\mathbf{N}_k^{(j-1)}$  where  $0 \leq j \leq n-r$ .

Substituting (27) in (25) yields

$$\mathbf{A}_{1:k} \mathbf{N}_k^{(0)-1} \mathbf{A}_{1:k}^{\top} = \mathbf{R}_k \mathbf{A}_{1:k-1} \mathbf{N}_{k-1}^{(n-r)-1} \mathbf{A}_{1:k-1}^{\top} \mathbf{R}_k^{\top} + \mathbf{K}_k \quad (28)$$

Let us define another ( $m \times m$ ) matrix  $\Psi_k^{(j)} \triangleq \mathbf{A}_{1:k} \mathbf{N}_k^{(j)-1} \mathbf{A}_{1:k}^{\top}$ , then (28) will be

$$\Psi_k^{(0)} = \mathbf{R}_k \Psi_{k-1}^{(n-r)} \mathbf{R}_k^{\top} + \mathbf{K}_k \quad (29)$$

which is the FMS ‘time update’ equation and should be computed once at each Kalman filter time epoch. Using the rank one update formula in [2] one can derive a relationship between  $\Psi_k^{(j)}$  and  $\Psi_k^{(j-1)}$  as

$$\Psi_k^{(j)} = \Psi_k^{(j-1)} - \frac{\Psi_k^{(j-1)} \mathbf{J}_{k+1}^{(j)} \Psi_k^{(j-1)}}{1 + \text{tr}(\Psi_k^{(j-1)} \mathbf{J}_{k+1}^{(j)})} \quad (30)$$

which is defined as FMS ‘fault downdate’ equation and should be computed  $r$  times, which means downdating the FMS due to fault-free satellites. The derivations of the fault downdate expression in (30) is given in Appendix B in details.

The worst-case FMS  $\rho_k^{*2} = \mathbf{t}_\varepsilon \Psi_k^{(0)} \mathbf{t}_\varepsilon^{\top}$  can be sequentially propagated using (29) and (30) with proper initial conditions. Using (15), (16),(17), and (27),  $\mathbf{B}_{0:0} = \mathbf{T}_0$  and  $\mathbf{A}_{0:0} = \mathbf{A}_{00} = \mathbf{L}_0 \mathbf{T}_0$  at  $k=0$ , therefore the initial condition will be

$$\Psi_0^{(0)} = \mathbf{L}_0 \mathbf{T}_0 (\mathbf{T}_0^{\top} \mathbf{S}_0^{-1} \mathbf{T}_0)^{-1} \mathbf{T}_0^{\top} \mathbf{L}_0^{\top} \quad (31)$$

### A. Fault Exclusion Capability of Innovation Sequence Monitor

Innovations sequence monitors when used with a single Kalman filter, does not have the capability of excluding the subset measurements associated with the fault. To bring the fault exclusion capability to the system, multi-hypothesis solution separation monitors (MHSS) that uses multiple sub-filters, is usually implemented. Such monitors can detect and isolate the measurements when detected, however it comes with the computational cost of sub filters. This section discusses the opportunity of utilizing the sequential FMS approach in bringing exclusion capability although using a single filter.

Recall that in the sequential FMS approach, both the time update and fault downdate recursions are established over the matrix  $\Psi_k$  that is computed for each fault hypothesis  $i$  ( $1 < i \leq n$ ). It was previously shown in [4] that the normalized failure mode slope  $\bar{\rho}_k^{(i)}$  for fault hypothesis  $i$  is linked to the standard deviation of solution separation  $\sigma_k^{(i)}$  and full-set solution  $\sigma_k^{(0)}$  (associated with the hazardous state  $\varepsilon_k$ ) for batch estimators as

$$\sigma_k^{(i)} = \sigma_k^{(0)} \sqrt{1 + \bar{\rho}_k^{(i)2}} \quad (32)$$

Substituting the failure mode slope  $\rho_k^* = \bar{\rho}_k \sigma_k^{(0)}$ , previously formulated as  $\rho_k^{*2} = \mathbf{t}_\varepsilon \Psi_k^{(0)} \mathbf{t}_\varepsilon^\top$ , into (34) yields:

$$\sigma_k^{(i)2} = \sigma_k^{(0)2} + \rho_k^{(i)2} \quad (33)$$

This relation is useful because the standard deviation of the solution separation can be obtained using a single filter with the sequential failure mode slope approach instead of running sub-filters. The standard deviations of the solution separations are used to compute the threshold for each test in MHSS. Using (33), one can extract the failure mode slope by  $\rho_k^{(i)2} = \mathbf{t}_\varepsilon \Psi_k \mathbf{t}_\varepsilon^\top$ , where recall the recursive equation for  $\Psi_k$  previously defined in (61) and (62) and  $\mathbf{t}_\varepsilon$  extracts the diagonal element in  $\Psi_k$  corresponding to the hazardous state. Given that information, one can generalize (33) as

$$\hat{\mathbf{P}}_k^{(i)} = \hat{\mathbf{P}}_k^{(0)} + \Psi_k \quad (34)$$

where  $\Psi_k$  corresponds to the difference between the sub-set and full-set covariances.

Using the same approach, one can also extract the solution separation, sub-set solutions  $\hat{\mathbf{x}}_k^{(i)}$ , which acts as the detection test statistic for MHSS, from a full-set solution  $\hat{\mathbf{x}}_k^{(0)}$  without needing to run parallel Kalman filters.

$$\hat{\mathbf{x}}_k^{(i)} = \hat{\mathbf{x}}_k^{(0)} - \frac{(\hat{\mathbf{P}}_k^{(0)} + \Psi_k) \mathbf{H}_k^{(i)\top} \gamma_k^{(i)}}{\sigma_k^{(i)2} - \alpha_k^2} \quad (35)$$

where  $\gamma_k^{(i)}$  ( $1 \times 1$ ) and  $\mathbf{H}_k^{(i)}$  ( $1 \times m$ ) are the innovation and observation matrix corresponding to the  $i^{\text{th}}$  measurement, respectively, and  $\alpha_k^2 = \mathbf{H}_k^{(i)} (\hat{\mathbf{P}}_k^{(0)} + \Psi_k) \mathbf{H}_k^{(i)\top}$  is a scalar. The derivation of (35) is provided in the Appendix C. (34) and (35) are computationally inexpensive way to obtain the sub-set solution without having to run sub-filters.

## VI. INNOVATION SEQUENCE BASED INTEGRITY MONITORING FOR INTEGRATED INS/GNSS NAVIGATION SYSTEMS

This section verifies, analyzes, and evaluates the proposed sequential integrity monitoring approach for a tightly coupled INS/GNSS system that is commonly used in aircraft navigation.

### A. Comparison of Block Matrix and Sequential Solutions to Failure Mode Slope

Using the sequential FMS approach, we compute the worst-case FMS and resulting integrity risk (due to a single satellite faults) values and compared them against the values obtained from the prior block matrix method. Prior fault, Kalman filter is assumed at steady-state with a tactical-grade inertial (STIM300) integrated to a differential GPS system with poor satellite geometry (i.e.,  $n = 4$ ). The poor satellite visibility scenario is intentionally selected to obtain non-zero integrity risk values for fair comparison. Table I shows the worst-case FMS values in degrees whereas Fig. 1 shows the resulting integrity risks for faults occurring for different time windows ranging from 2 min to approximately 3 min. In this example, we use an alert limit  $\ell = 10$  m, a prior fault probability  $P_H = 1$ , and a probability of false alarm  $P_{FA} = 10^{-6}$ . One can notice that the block matrix and sequential approach results are approximately the same, for example the integrity risk values are matching perfectly even in  $10^{-8}$  level.

TABLE I: Block vs sequential solution to worst-case FMS for STIM300 integrated with a differential GPS receiver

Post-Fault Monitoring, s	Worst-Case FMS, deg	
	Block Matrix	Sequential
120	20.223	20.223
128	23.062	23.063
136	26.029	26.030
144	29.091	29.092
152	32.211	32.213
160	35.351	35.353
168	38.473	38.475
176	41.542	41.544
184	44.528	44.530

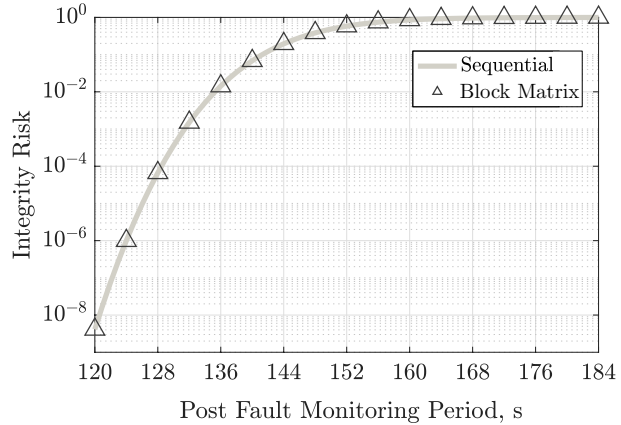


Fig. 1: Block vs sequential solution to integrity risk with  $\ell = 10$  m vertical alert limit and  $P_{FA} = 10^{-6}$  probability of false alarm.

### B. Effect of Satellite Geometry

For baseline ARAIM techniques, without the inertial aid, detection function is available only when there is satellite redundancy, that is  $n - r \geq 4$ . To investigate the effect of satellite redundancy on the proposed monitor performance, we simulate a fixed satellite geometry (i.e.,  $n = 6$ ) in the existence of worst-case faults where the number of faulty satellites varies as  $6 \geq r \geq 1$ . Fig. 2 shows the worst-case FMS for a GNSS receiver tightly-coupled to a navigation-grade IMU through a 5 min time window. As seen in the figure, for single and dual satellite fault hypothesis ( $r \leq 2$ ) where there is satellite redundancy, FMS levels off at small values less than  $10^\circ$ . This is because the redundant measurements reflect and accumulate in the test statistic over time, which ultimately overcomes the degrading effect of threshold increase, thereby the detection capability is preserved regardless of the fault duration. On the other hand, the figure also shows that for higher number of fault hypothesis ( $6 \geq r \geq 3$ ), FMS increases and ultimately converges to the highest value,  $90^\circ$  which is because there is no satellite redundancy. In such cases, inertial sensors resists to faults for a while, however it is ultimately corrupted in a tightly-coupled mechanism, thereby the monitor

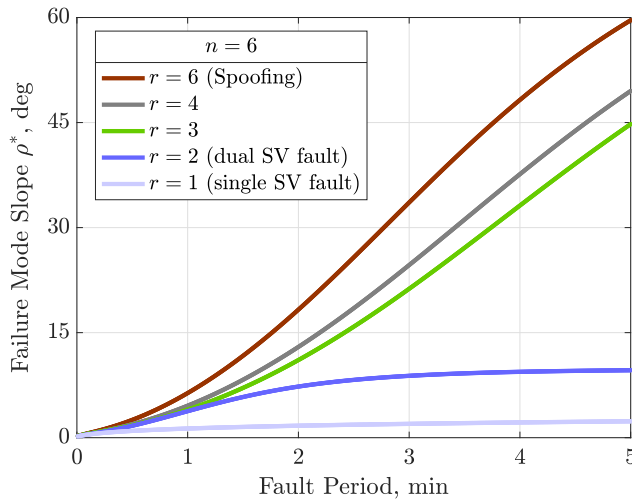


Fig. 2: The effect of satellite redundancy on the worst-case FMS.  $r$  is the number of faulty satellites,  $n$  is the number of total visible satellites.

loses its detection capability over time.

### C. Factor of Inertial Sensor Quality

The integrity performance of the monitor is quantified using different inertial sensors including generic automotive-grade (AUTO), low/high-end tactical-grades (LTAC/HTAC), navigation-grade (NAV), as well as a commonly used specific one, STIM300, specifications of which is presented in Table II.

TABLE II: Examples of Different Quality IMU Sensor Specifications

	AUTO	LTAC	STIM300	HTAC	NAV	Units
Sampling interval	10.0	10.0	8.0	10	10	ms
Bias Time Constant	1	1	1	1	1	hr
Gyro Bias Stability	100	10	0.5	0.1	0.01	deg/hr
Gyro Bias Repeatability	1000	100	4.0	1.0	0.1	deg/hr
Acceleration Bias Stability	10.0	1	0.05	0.2	0.010	mg
Acceleration Bias Repeatability	100	10.0	0.75	2.0	0.1	mg
Angular Random Walk	3	0.6	0.15	0.06	0.0018	deg/ $\sqrt{\text{hr}}$
Velocity Random Walk	0.1174	0.0587	0.07	0.0293	0.0018	m/s/ $\sqrt{\text{hr}}$

Using the inertial specifications, the worst-case FMS are propagated through a 90 min single satellite fault when there are 6 and 5 satellites in view in Figure 3. Both of the scenarios have satellite redundancy for detection, therefore regardless of the inertial quality the worst-case FMS converges to small values (less than  $2^\circ$ ) which results in zero integrity risks in the simulations. This is because the satellite redundancy provides sufficient information for detection without needing use of inertial sensor measurements. To clearly see the difference in the monitor performance when used with and without inertial sensors, we simulate a scenario where an infinite process noise is fed into Kalman filter (equivalent to use of a dummy inertial sensor). The resulting worst-case FMS is shown with the hatched black curve, which as seen in the figure, is very close to those obtained when used with different quality inertial sensors. The integrity risk resulting from the dummy inertial simulation is still zero, which explicitly suggests that the real value of inertial sensors in the proposed monitor is primarily to preserve navigation integrity through a temporary poor satellite visibility condition.

To investigate the worst-case FMS characteristic in the existence of no satellite redundancy, where baseline ARAIM is disabled, we simulated scenarios in Fig 4, where the monitor's resistance to faults are quantified for use of different quality inertial sensors. In the figure, one can clearly notice that the inertial quality affects the worst-case FMS and the associated integrity risks drastically. For example, the integrity risk immediately reaches to 1 when

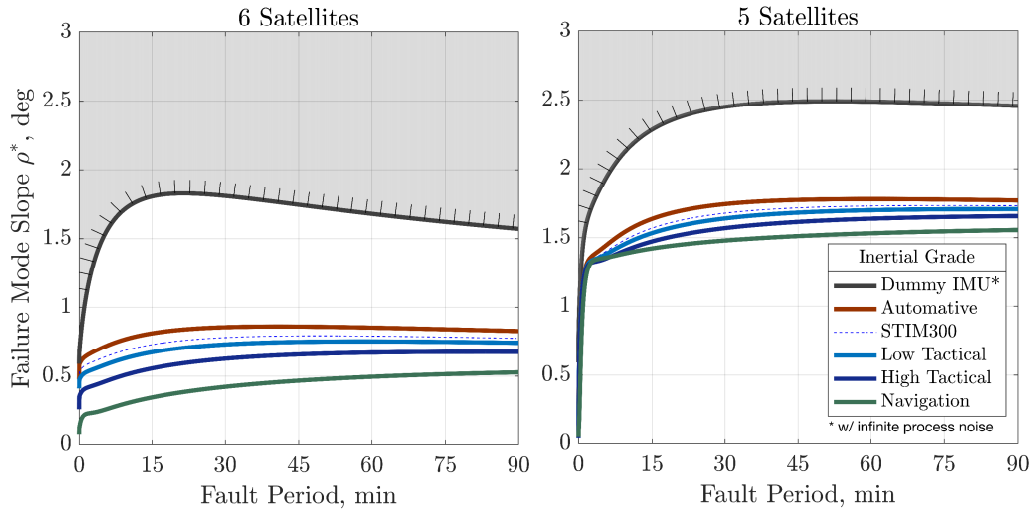


Fig. 3: The effect of inertial quality on the worst-case FMS in the existing of satellite redundancy

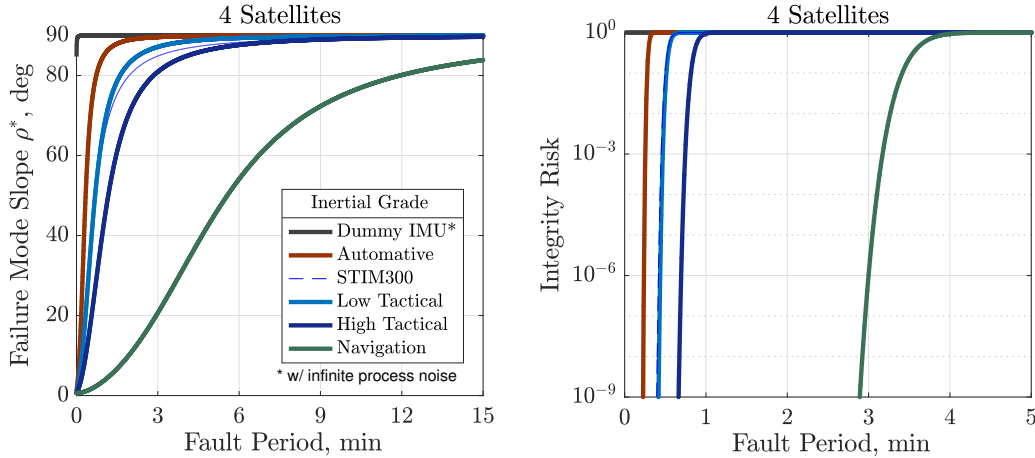


Fig. 4: The effect of inertial quality when satellite redundancy is unavailable.

the proposed monitor is used without an inertial sensor (dummy inertial case) whereas it reaches to 1 only after 3 min when it is used with a navigation-grade inertial sensor.

#### D. Integrity Performance in Aircraft En Route, Approach, and Landing Operations

The analyses in Sections VI-B and VI-C suggest that the proposed monitor provides high integrity in the existence of satellite redundancy, as well as depending on the inertial quality, has a potential of preserving integrity for limited time periods in the existence of low satellite visibility. This section demonstrates the feasibility of the monitor for the use on aircraft equipped with navigation-grade inertials, against worst-case single satellite faults during en route and approach operations, requirements of which are listed in Table III. The table contains both the vertical and horizontal alert limits and the associated navigation integrity and continuity requirements per operation. For each operation, the test statistic threshold ( $T$ ) is computed using the continuity risk requirements in the table.

TABLE III: Aircraft en route and approach navigation continuity and integrity requirements

Operation Type	Vertical $\ell$	Horizontal $\ell$	Integrity Risk	Continuity Risk
LPV 200 Approach	35 m	40 m	$10^{-7}/150s$	$10^{-6}/150s$
CAT I Precision Approach	10 m	40 m	$2 \times 10^{-7}/150s$	$10^{-6}/150s$
CAT II-III Precision Approach	5.3 m	17 m	$10^{-9}/150s$	$10^{-6}/150s$
RNP 0.1 En Route Terminal	—	185 m	$10^{-7}/hr$	$10^{-8}/hr$
RNP 0.3 En Route Oceanic	—	556 m	$10^{-7}/hr$	$10^{-8}/hr$

The covariance analyses with  $n \geq 5$ , yield zero integrity risks for all of the operations including the most stringent CAT-II/III vertical precision approach and RNP 0.1 terminal en route. This is remarkable because the snapshot A-RAIM techniques achieve meeting only the LPV200 approach requirement. Under poor visibility ( $n = 4$ ), where baseline ARAIM is unavailable, the proposed monitor with the aid of inertial, meets integrity requirements of all operations except CAT-II/III vertical precision approach, RNP 0.1 and RNP 0.3 en route missions. For these categories, we quantified how long the proposed monitor can maintain navigation integrity through a potential poor visibility condition without exceeding the requirements. Fig. 5 shows the horizontal integrity risk during 60 min RNP 0.1 and RNP 0.3 en route operations whereas Fig. 6 presents vertical integrity risk during a 150 s CAT-II/III precision approach. For fixed satellite geometry scenario, the integrity risk curves (blue) remain within the required region (below the dashed lines) for approximately 23 min for RNP 0.1, 37 min for RNP 0.3, and 136 s for CAT-II/III.

Recall that unlike snapshot A-RAIM, the proposed monitor exploits changes in satellite geometry. From the perspective of a user on earth, the satellite motion is small over less-than-ten-minute-long time intervals [6], however the accumulated geometry variations over longer time can be substantial especially in en route aircraft operations. To quantify the leveraging effect of satellite motion, two scenario results one with frozen satellite geometry (time

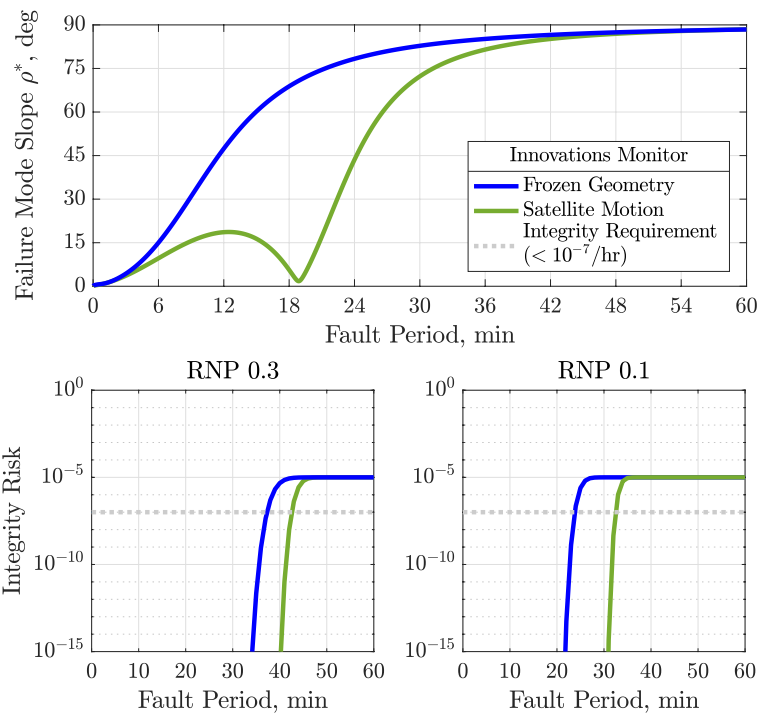


Fig. 5: The worst-case FMS and associated integrity risk with RNP 0.1 en route terminal and RNP 0.3 en route oceanic operation requirements in the absence of satellite redundancy.

invariant–blue curves) another with satellite motion (time variant–green curves), are compared. As seen in Fig 5, satellite motion appears as a fluctuation in the worst-case FMS, which causes a reasonable delay in its convergence to high slopes, thereby a time shift in the integrity risk curves to the right. For example, by means of satellite motion the time period of guaranteed horizontal positioning integrity is extended by approximately 6 min for RNP

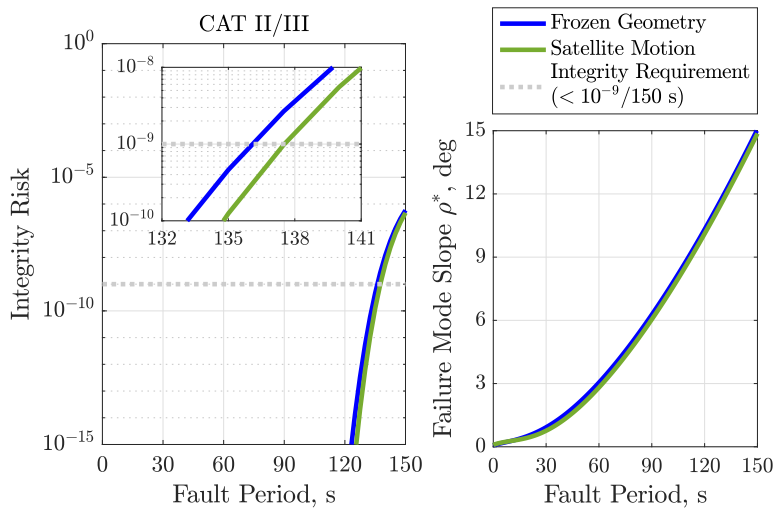


Fig. 6: The worst-case FMS and associated integrity risk with CAT II/III (vertical) precision approach requirements in the absence of satellite redundancy.

0.1 and 10 min for RNP 0.3, which is approximately 27% improvement in the integrity. Its effect is negligible for CAT II/III precision approaches, approximately a 1 s extension in the preserved integrity window (Fig. 6), which is expected because satellite geometry variations are small over a standard approach time (150 s).

## VII. CONCLUSION

This paper derives, analyzes, and evaluates a novel time-sequential integrity monitoring technique that is capable of detecting and excluding faults using a single Kalman filter. Its performance against worst-case single satellite faults is verified on tightly-coupled INS/GNSS navigation systems used during safety-critical aircraft en route and approach operations. It is demonstrated that its integrity performance is superior to conventional snapshot ARAIM techniques, providing guaranteed integrity even for the most stringent operation requirements (e.g., CAT II/III precision approach and RNP 0.1 terminal en route). It is also shown that for temporary poor satellite visibility conditions, when baseline A-RAIM is unavailable, the proposed monitor with the aid of inertial sensor measurements, still preserves protection levels for reasonable time periods.

### APPENDIX A FAILURE MODE SLOPE TIME UPDATE

This section presents the derivation of Eq. (25) used in the FMS time update equation derivations in Sect. V. Using (23) and (24), the recursive form of  $\bar{\mathbf{B}}_{1:k}^T \mathbf{S}_{1:k}^{-1} \bar{\mathbf{B}}_{1:k}$  will be

$$\begin{aligned} \bar{\mathbf{B}}_{1:k}^T \mathbf{S}_{1:k}^{-1} \bar{\mathbf{B}}_{1:k} &= \begin{bmatrix} \bar{\mathbf{B}}_{1:k-1}^T & -\mathbf{A}_{1:k-1}^T \Phi_k^T \mathbf{H}_k^T \\ \mathbf{0} & \mathbf{T}_k^T \end{bmatrix} \begin{bmatrix} \mathbf{S}_{1:k-1}^{-1} & \mathbf{0} \\ \mathbf{0} & \mathbf{S}_k^{-1} \end{bmatrix} \begin{bmatrix} \bar{\mathbf{B}}_{1:k-1} & \mathbf{0} \\ -\mathbf{H}_k \Phi_k \mathbf{A}_{1:k-1} & \mathbf{T}_k \end{bmatrix} \\ &= \begin{bmatrix} \bar{\mathbf{B}}_{1:k-1}^T \mathbf{S}_{1:k-1}^{-1} \bar{\mathbf{B}}_{1:k-1} + \mathbf{A}_{1:k-1}^T \Phi_k^T \mathbf{H}_k^T \mathbf{S}_k^{-1} \mathbf{H}_k \Phi_k \mathbf{A}_{1:k-1} & -\mathbf{A}_{1:k-1}^T \Phi_k^T \mathbf{H}_k^T \mathbf{S}_k^{-1} \mathbf{T}_k \\ -\mathbf{T}_k^T \mathbf{S}_k^{-1} \mathbf{H}_k \Phi_k \mathbf{A}_{1:k-1} & \mathbf{T}_k^T \mathbf{S}_k^{-1} \mathbf{T}_k \end{bmatrix} \end{aligned} \quad (36)$$

To invert (36), one can use block matrix inversion lemma [3]:

$$\begin{bmatrix} \Delta & \Gamma \\ \Theta & \Lambda \end{bmatrix}^{-1} = \begin{bmatrix} (\Delta - \Gamma \Lambda^{-1} \Theta)^{-1} & -(\Delta - \Gamma \Lambda^{-1} \Theta)^{-1} \Gamma \Lambda^{-1} \\ -\Lambda^{-1} \Theta (\Delta - \Gamma \Lambda^{-1} \Theta)^{-1} & \Lambda^{-1} + \Lambda^{-1} \Theta (\Delta - \Gamma \Lambda^{-1} \Theta)^{-1} \Gamma \Lambda^{-1} \end{bmatrix} \quad (37)$$

Comparing the terms in (36) and (37), one can obtain:

$$\Lambda^{-1} = (\mathbf{T}_k^T \mathbf{S}_k^{-1} \mathbf{T}_k)^{-1} \quad (38)$$

$$\Theta = -\mathbf{T}_k^T \mathbf{S}_k^{-1} \mathbf{H}_k \Phi_k \mathbf{A}_{1:k-1} \quad (39)$$

$$\Gamma = -\mathbf{A}_{1:k-1}^T \Phi_k^T \mathbf{H}_k^T \mathbf{S}_k^{-1} \mathbf{T}_k \quad (40)$$

Using (38), (39), and (40):

$$\begin{aligned} (\Delta - \Gamma \Lambda^{-1} \Theta)^{-1} \triangleq \mathbf{M}_{k-1}^{-1} &= \left[ \bar{\mathbf{B}}_{1:k-1}^T \mathbf{S}_{1:k-1}^{-1} \bar{\mathbf{B}}_{1:k-1} + \mathbf{A}_{1:k-1}^T \Phi_k^T \mathbf{H}_k^T \mathbf{S}_k^{-1} \mathbf{H}_k \Phi_k \mathbf{A}_{1:k-1} \right. \\ &\quad \left. - \mathbf{A}_{1:k-1}^T \Phi_k^T \mathbf{H}_k^T \mathbf{S}_k^{-1} \mathbf{T}_k (\mathbf{T}_k^T \mathbf{S}_k^{-1} \mathbf{T}_k)^{-1} \mathbf{T}_k^T \mathbf{S}_k^{-1} \mathbf{H}_k \Phi_k \mathbf{A}_{1:k-1} \right]^{-1} \end{aligned} \quad (41)$$

or

$$\mathbf{M}_{k-1}^{-1} = \left[ \bar{\mathbf{B}}_{1:k-1}^T \mathbf{S}_{1:k-1}^{-1} \bar{\mathbf{B}}_{1:k-1} + \mathbf{A}_{1:k-1}^T \Phi_k^T \mathbf{H}_k^T \mathbf{S}_k^{-1} \left\{ \mathbf{I} - \mathbf{T}_k (\mathbf{T}_k^T \mathbf{S}_k^{-1} \mathbf{T}_k)^{-1} \mathbf{T}_k^T \mathbf{S}_k^{-1} \right\} \mathbf{H}_k \Phi_k \mathbf{A}_{1:k-1} \right]^{-1} \quad (42)$$

Recall that the second term inside the inverse parenthesis in (42) has a rank of  $n - r$  and represents the effect of fault-free satellites on the FMS. The more fault-free measurement the less FMS will be because of the inverse relation. Notice that for full-set measurement faults,  $\mathbf{T}_k = \mathbf{I}$ , therefore the highlighted term (or the second term) will cancel out, which would yield a direct recursive relation between  $(\bar{\mathbf{B}}_{1:k}^T \mathbf{S}_{1:k}^{-1} \bar{\mathbf{B}}_{1:k})^{-1}$  and  $(\bar{\mathbf{B}}_{1:k-1}^T \mathbf{S}_{1:k-1}^{-1} \bar{\mathbf{B}}_{1:k-1})^{-1}$  because  $\mathbf{M}_{k-1}^{-1} = (\bar{\mathbf{B}}_{1:k-1}^T \mathbf{S}_{1:k-1}^{-1} \bar{\mathbf{B}}_{1:k-1})^{-1}$ .

Similarly,

$$-(\Delta - \Gamma\Lambda^{-1}\Theta)^{-1}\Gamma\Lambda^{-1} = \mathbf{M}_{k-1}^{-1}\mathbf{A}_{1:k-1}^\top\Phi_k^\top\mathbf{H}_k^\top\mathbf{T}_k \quad (43)$$

$$-\Lambda^{-1}\Theta(\Delta - \Gamma\Lambda^{-1}\Theta)^{-1} = \mathbf{T}_k^\top\mathbf{H}_k\Phi_k\mathbf{A}_{1:k-1}\mathbf{M}_{k-1}^{-1} \quad (44)$$

$$\Lambda^{-1} + \Lambda^{-1}\Theta(\Delta - \Gamma\Lambda^{-1}\Theta)^{-1}\Gamma\Lambda^{-1} = (\mathbf{T}_k^\top\mathbf{S}_k^{-1}\mathbf{T}_k)^{-1} + \mathbf{T}_k^\top\mathbf{H}_k\Phi_k\mathbf{A}_{1:k-1}\mathbf{M}_{k-1}^{-1}\mathbf{A}_{1:k-1}^\top\mathbf{H}_k^\top\Phi_k^\top\mathbf{T}_k \quad (45)$$

Substituting (43), (44), (45), and (42) into (37) gives

$$(\overline{\mathbf{B}}_{1:k}^\top\mathbf{S}_{1:k}^{-1}\overline{\mathbf{B}}_{1:k})^{-1} = \begin{bmatrix} \mathbf{M}_{k-1}^{-1} & \mathbf{M}_{k-1}^{-1}\mathbf{A}_{1:k-1}^\top\Phi_k^\top\mathbf{H}_k^\top\mathbf{T}_k \\ \mathbf{T}_k^\top\mathbf{H}_k\Phi_k\mathbf{A}_{1:k-1}\mathbf{M}_{k-1}^{-1} & (\mathbf{T}_k^\top\mathbf{S}_k^{-1}\mathbf{T}_k)^{-1} + \mathbf{T}_k^\top\mathbf{H}_k\Phi_k\mathbf{A}_{1:k-1}\mathbf{M}_{k-1}^{-1}\mathbf{A}_{1:k-1}^\top\Phi_k^\top\mathbf{H}_k^\top\mathbf{T}_k \end{bmatrix} \quad (46)$$

where  $\mathbf{M}_{k-1}^{-1}$  is  $r(k-1) \times r(k-1)$ ,  $\mathbf{A}_{k-1}$  is  $m \times r(k-1)$ , and  $\overline{\mathbf{B}}_{1:k}^\top\mathbf{S}_{1:k}^{-1}\overline{\mathbf{B}}_{1:k}$  is  $rk \times rk$ .

To obtain worst-case slope expression, substitute (22) and (46) into (21):

$$\begin{aligned} \mathbf{A}_{1:k}(\overline{\mathbf{B}}_{1:k}^\top\mathbf{S}_{1:k}^{-1}\overline{\mathbf{B}}_{1:k})^{-1}\mathbf{A}_{1:k}^\top &= [(\mathbf{I} - \mathbf{L}_k\mathbf{H}_k)\Phi_k\mathbf{A}_{1:k-1} \quad \mathbf{L}_k\mathbf{T}_k] \\ &\times \begin{bmatrix} \mathbf{M}_{k-1}^{-1} & \mathbf{M}_{k-1}^{-1}\mathbf{A}_{1:k-1}^\top\Phi_k^\top\mathbf{H}_k^\top\mathbf{T}_k \\ \mathbf{T}_k^\top\mathbf{H}_k\Phi_k\mathbf{A}_{1:k-1}\mathbf{M}_{k-1}^{-1} & (\mathbf{T}_k^\top\mathbf{S}_k^{-1}\mathbf{T}_k)^{-1} + \mathbf{T}_k^\top\mathbf{H}_k\Phi_k\mathbf{A}_{1:k-1}\mathbf{M}_{k-1}^{-1}\mathbf{A}_{1:k-1}^\top\Phi_k^\top\mathbf{H}_k^\top\mathbf{T}_k \end{bmatrix} \\ &\times \begin{bmatrix} \mathbf{A}_{1:k-1}^\top\Phi_k^\top(\mathbf{I} - \mathbf{H}_k^\top\mathbf{L}_k^\top) \\ \mathbf{T}_k^\top\mathbf{L}_k^\top \end{bmatrix} \\ &= (\mathbf{I} - \mathbf{L}_k\mathbf{H}_k + \mathbf{L}_k\mathbf{T}_k\mathbf{T}_k^\top\mathbf{H}_k)\Phi_k\mathbf{A}_{1:k-1}\mathbf{M}_{k-1}^{-1}\mathbf{A}_{1:k-1}^\top\Phi_k^\top(\mathbf{I} - \mathbf{L}_k\mathbf{H}_k + \mathbf{L}_k\mathbf{T}_k\mathbf{T}_k^\top\mathbf{H}_k)^\top \\ &\quad + \mathbf{L}_k\mathbf{T}_k(\mathbf{T}_k^\top\mathbf{S}_k^{-1}\mathbf{T}_k)^{-1}\mathbf{T}_k^\top\mathbf{L}_k^\top \end{aligned} \quad (47)$$

Recall  $\mathbf{M}_{k-1}^{-1}$  was previously found as

$$\mathbf{M}_{k-1}^{-1} = \left[ \overline{\mathbf{B}}_{1:k-1}^\top\mathbf{S}_{1:k-1}^{-1}\overline{\mathbf{B}}_{1:k-1} + \mathbf{A}_{1:k-1}^\top\Phi_k^\top\mathbf{H}_k^\top\mathbf{S}_k^{-1}\{\mathbf{I} - \mathbf{T}_k(\mathbf{T}_k^\top\mathbf{S}_k^{-1}\mathbf{T}_k)^{-1}\mathbf{T}_k^\top\mathbf{S}_k^{-1}\}\mathbf{H}_k\Phi_k\mathbf{A}_{1:k-1} \right]^{-1} \quad (48)$$

For the simplicity let us define an  $(m \times m)$  matrices

$$\mathbf{J}_k \triangleq \Phi_k^\top\mathbf{H}_k^\top\mathbf{S}_k^{-1}[\mathbf{I} - \mathbf{T}_k(\mathbf{T}_k^\top\mathbf{S}_k^{-1}\mathbf{T}_k)^{-1}\mathbf{T}_k^\top\mathbf{S}_k^{-1}]\mathbf{H}_k\Phi_k, \quad (49)$$

$$\mathbf{R}_k \triangleq (\mathbf{I} - \mathbf{L}_k\mathbf{H}_k + \mathbf{L}_k\mathbf{T}_k\mathbf{T}_k^\top\mathbf{H}_k)\Phi_k, \quad (50)$$

$$\mathbf{K}_k \triangleq \mathbf{L}_k\mathbf{T}_k(\mathbf{T}_k^\top\mathbf{S}_k^{-1}\mathbf{T}_k)^{-1}\mathbf{T}_k^\top\mathbf{L}_k^\top, \quad (51)$$

then (48) and (47) can be re-written as

$$\mathbf{M}_{k-1}^{-1} = (\overline{\mathbf{B}}_{1:k-1}^\top\mathbf{S}_{1:k-1}^{-1}\overline{\mathbf{B}}_{1:k-1} + \mathbf{A}_{1:k-1}^\top\mathbf{J}_k\mathbf{A}_{1:k-1})^{-1} \quad (52)$$

$$\mathbf{A}_{1:k}(\overline{\mathbf{B}}_{1:k}^\top\mathbf{S}_{1:k}^{-1}\overline{\mathbf{B}}_{1:k})^{-1}\mathbf{A}_{1:k}^\top = \mathbf{R}_k\mathbf{A}_{1:k-1}\mathbf{M}_{k-1}^{-1}\mathbf{A}_{1:k-1}^\top\mathbf{R}_k^\top + \mathbf{K}_k \quad (53)$$

Substituting (52) into (53) yields:

$$\mathbf{A}_{1:k}(\overline{\mathbf{B}}_{1:k}^\top\mathbf{S}_{1:k}^{-1}\overline{\mathbf{B}}_{1:k})^{-1}\mathbf{A}_{1:k}^\top = \mathbf{R}_k\mathbf{A}_{1:k-1}(\overline{\mathbf{B}}_{1:k-1}^\top\mathbf{S}_{1:k-1}^{-1}\overline{\mathbf{B}}_{1:k-1} + \mathbf{A}_{1:k-1}^\top\mathbf{J}_k\mathbf{A}_{1:k-1})^{-1}\mathbf{A}_{1:k-1}^\top\mathbf{R}_k^\top + \mathbf{K}_k \quad (54)$$

$$(55)$$

Note that the inverse parenthesis term,  $(\mathbf{T}_k^\top\mathbf{S}_k^{-1}\mathbf{T}_k)^{-1}$ , in (49) will be one dimensional simple inversion for a single measurement fault hypothesis, i.e.  $r = 1$ .

APPENDIX B  
FAILURE MODE SLOPE FAULT DOWNDATE

This section presents the fault downdate derivation steps between (28) and (30) in Sect V. Recall (56) and (28):

$$\mathbf{N}_k^{(i)} \triangleq \begin{cases} \overline{\mathbf{B}}_{1:k}^\top \mathbf{S}_{1:k}^{-1} \overline{\mathbf{B}}_{1:k} + \sum_{j=1}^i \mathbf{A}_{1:k}^\top \mathbf{J}_{k+1}^{(j)} \mathbf{A}_{1:k} & \text{if } i > 0 \\ \overline{\mathbf{B}}_{1:k}^\top \mathbf{S}_{1:k}^{-1} \overline{\mathbf{B}}_{1:k} & \text{if } i = 0 \end{cases} \quad (56)$$

$$\mathbf{A}_{1:k} \mathbf{N}_k^{(0)-1} \mathbf{A}_{1:k}^\top = \mathbf{R}_k \mathbf{A}_{1:k-1} \mathbf{N}_{k-1}^{(n-r)-1} \mathbf{A}_{1:k-1}^\top \mathbf{R}_k^\top + \mathbf{K}_k \quad (57)$$

where  $\mathbf{N}_k^{(j)}$  is rank-1 update of  $\mathbf{N}_k^{(j-1)}$  where  $0 \leq j \leq n-r$ . Therefore, the relation between their inverses will be [2]:

$$\mathbf{N}_k^{(j)-1} = (\mathbf{N}_k^{(j-1)} + \mathbf{A}_{1:k}^\top \mathbf{J}_{k+1}^{(j)} \mathbf{A}_{1:k})^{-1} = \mathbf{N}_k^{(j-1)-1} - \frac{\mathbf{N}_k^{(j-1)-1} \mathbf{A}_{1:k}^\top \mathbf{J}_{k+1}^{(j)} \mathbf{A}_{1:k} \mathbf{N}_k^{(j-1)-1}}{1 + \text{tr}(\mathbf{A}_{1:k}^\top \mathbf{J}_{k+1}^{(j)} \mathbf{A}_{1:k} \mathbf{N}_k^{(j-1)-1})} \quad (58)$$

where using switching property of the trace operator, (58) can be re-written as:

$$\mathbf{N}_k^{(j)-1} = \mathbf{N}_k^{(j-1)-1} - \frac{\mathbf{N}_k^{(j-1)-1} \mathbf{A}_{1:k}^\top \mathbf{J}_{k+1}^{(j)} \mathbf{A}_{1:k} \mathbf{N}_k^{(j-1)-1}}{1 + \text{tr}(\mathbf{A}_{1:k} \mathbf{N}_k^{(j-1)-1} \mathbf{A}_{1:k}^\top \mathbf{J}_{k+1}^{(j)})}. \quad (59)$$

Post- and pre-multiplying (59) with  $\mathbf{A}_{1:k}$  and  $\mathbf{A}_{1:k}^\top$ , respectively, gives:

$$\mathbf{A}_{1:k} \mathbf{N}_k^{(j)-1} \mathbf{A}_{1:k}^\top = \mathbf{A}_{1:k} \mathbf{N}_k^{(j-1)-1} \mathbf{A}_{1:k}^\top - \frac{\mathbf{A}_{1:k} \mathbf{N}_k^{(j-1)-1} \mathbf{A}_{1:k}^\top \mathbf{J}_{k+1}^{(j)} \mathbf{A}_{1:k} \mathbf{N}_k^{(j-1)-1} \mathbf{A}_{1:k}^\top}{1 + \text{tr}(\mathbf{A}_{1:k} \mathbf{N}_k^{(j-1)-1} \mathbf{A}_{1:k}^\top \mathbf{J}_{k+1}^{(j)})} \quad (60)$$

Recall the previous definition in Sect. V:  $\Psi_k^{(j)} \triangleq \mathbf{A}_{1:k} \mathbf{N}_k^{(j)-1} \mathbf{A}_{1:k}^\top$ , of which size is bounded by  $(m \times m)$  over time. Then re-expressing (53) yields time update recursive equation as

$$\Psi_k^{(0)} = \mathbf{R}_k \Psi_{k-1}^{(n-r)} \mathbf{R}_k^\top + \mathbf{K}_k \quad (61)$$

and similarly re-expressing (60) gives measurement fault downdate recursive equation as:

$$\Psi_k^{(j)} = \Psi_k^{(j-1)} - \frac{\Psi_k^{(j-1)} \mathbf{J}_{k+1}^{(j)} \Psi_k^{(j-1)}}{1 + \text{tr}(\Psi_k^{(j-1)} \mathbf{J}_{k+1}^{(j)})} \quad (62)$$

where recall that subscript  $k$  and superscript  $(j)$  represent time update and fault downdate recursions, respectively.

One can notice that (61) and (62) will be trivial for full-set measurement faults, that is  $\mathbf{T}_k = \mathbf{I}$ , for example GNSS spoofing attack where all the receiver channels are spoofed. In that case, the second term on the right hand side of (62) will be zero, therefore the only recursion will be through (61). Furthermore, substituting  $\mathbf{T}_k = \mathbf{I}$  into (49) and (51) gives:

$$\mathbf{K}_k = \mathbf{L}_k \mathbf{S}_k \mathbf{L}_k^\top \quad (63)$$

and

$$\mathbf{R}_k = \mathbf{C}_k + \mathbf{L}_k \mathbf{H}_k \Phi_k = (\mathbf{I} - \mathbf{L}_k \mathbf{H}_k) \Phi_k + \mathbf{L}_k \mathbf{H}_k \Phi_k = \Phi_k. \quad (64)$$

Substituting these into (61) yields the recursive slope equation for full-set measurement faults as

$$\Psi_k = \Phi_k \Psi_{k-1} \Phi_k^\top + \mathbf{L}_k \mathbf{S}_k \mathbf{L}_k^\top \quad (65)$$

APPENDIX C  
OBTAINING SOLUTION SEPARATIONS FROM FULL-SET SOLUTION

Let  $\hat{\mathbf{x}}_k^{(0)}$  be the state estimate at epoch  $k$  using full-set measurements, using sequential measurement update method it is related to the state estimate  $\hat{\mathbf{x}}_k^{(i)}$  obtained from a subset measurements (measurement  $i$  excluded) as

$$\begin{aligned}\hat{\mathbf{x}}_k^{(0)} &= \hat{\mathbf{x}}_k^{(i)} + \mathbf{L}_k^{(i)} (z_k^{(i)} - \mathbf{H}_k^{(i)} \hat{\mathbf{x}}_k^{(i)}) \\ &= (\mathbf{I} - \mathbf{L}_k^{(i)} \mathbf{H}_k^{(i)}) \hat{\mathbf{x}}_k^{(i)} + \mathbf{L}_k^{(i)} z_k^{(i)}\end{aligned}\quad (66)$$

where assuming single measurement fault hypothesis,  $\mathbf{L}_k^{(i)}$  ( $m \times 1$ ),  $\mathbf{H}_k^{(i)}$  ( $1 \times m$ ) are the Kalman gain and observation matrices corresponding to the  $i$ th measurement update, and  $z_k^{(i)}$  ( $1 \times 1$ ) is the  $i$ th measurement. Rearranging (66)

$$\hat{\mathbf{x}}_k^{(i)} = (\mathbf{I} - \mathbf{L}_k^{(i)} \mathbf{H}_k^{(i)})^{-1} (\hat{\mathbf{x}}_k^{(0)} - \mathbf{L}_k^{(i)} z_k^{(i)}) \quad (67)$$

where using matrix inversion lemma,  $(\mathbf{I} + \mathbf{u}\mathbf{v}^\top)^{-1} = \mathbf{I} - \mathbf{u}\mathbf{v}^\top / (1 + \mathbf{v}^\top \mathbf{u})$ , the  $(m \times m)$  inversion term in (68) can be reduced to form that only contains one-dimensional inversion as

$$\hat{\mathbf{x}}_k^{(i)} = \left( \mathbf{I} + \frac{\mathbf{L}_k^{(i)} \mathbf{H}_k^{(i)}}{1 - \mathbf{H}_k^{(i)} \mathbf{L}_k^{(i)}} \right) (\hat{\mathbf{x}}_k^{(0)} - \mathbf{L}_k^{(i)} z_k^{(i)}) \quad (68)$$

where  $\mathbf{L}_k^{(i)}$  is a function of solution separation covariance  $\hat{\mathbf{P}}_k^{(i)}$  as

$$\mathbf{L}_k^{(i)} = \frac{\hat{\mathbf{P}}_k^{(i)} \mathbf{H}_k^{(i)\top}}{\sigma_k^{(i)2}} = \frac{(\hat{\mathbf{P}}_k^{(0)} + \mathbf{\Psi}_k) \mathbf{H}_k^{(i)\top}}{\sigma_k^{(i)2}} \quad (69)$$

where  $\sigma_k^{(i)}$  is the standard deviation of  $z_k^{(i)}$ .

Let us define a scalar  $\alpha_k^2 = \mathbf{H}_k^{(i)} (\hat{\mathbf{P}}_k^{(0)} + \mathbf{\Psi}_k) \mathbf{H}_k^{(i)\top}$ , then using (69) and (68) one can obtain solution separation as:

$$\hat{\mathbf{x}}_k^{(i)} = \hat{\mathbf{x}}_k^{(0)} - \frac{(\hat{\mathbf{P}}_k^{(0)} + \mathbf{\Psi}_k) \mathbf{H}_k^{(i)\top} (z_k^{(i)} - \mathbf{H}_k^{(i)} \hat{\mathbf{x}}_k^{(0)})}{\sigma_k^{(i)2} - \alpha_k^2} \quad (70)$$

or by replacing innovation  $\gamma_k^{(i)} = z_k^{(i)} - \mathbf{H}_k^{(i)} \hat{\mathbf{x}}_k^{(0)}$ :

$$\hat{\mathbf{x}}_k^{(i)} = \hat{\mathbf{x}}_k^{(0)} - \frac{(\hat{\mathbf{P}}_k^{(0)} + \mathbf{\Psi}_k) \mathbf{H}_k^{(i)\top} \gamma_k^{(i)}}{\sigma_k^{(i)2} - \alpha_k^2}. \quad (71)$$

REFERENCES

- [1] C. Tanil, S. Khanafseh, M. Joerger, B. Pervan, "An INS Monitor to Detect GNSS Spoofers Capable of Tracking Aircraft Position," *IEEE Transactions on Aerospace and Electronics*, vol. 54, no. 1, pp. 131–143, Feb 2018.
- [2] K. S. Miller, "On the Inverse of the Sum of Matrices," *JSTOR Mathematics Magazine*, vol. 54, no. 2, pp. 62–72, 1981.
- [3] J. Sherman, W. J. Morrison, "Adjustment of an Inverse Matrix Corresponding to Changes in the Elements of a Given Column or a Given Row of the Original Matrix," *Annals of Mathematical Statistics*, vol. 54, no. 20, pp. 621, 1949.
- [4] M. Joerger, F.-C. Chan, and B. Pervan, "Solution Separation Versus Residual-Based RAIM," *NAVIGATION, Journal of The Institute of Navigation*, vol. 61, no. 4, 2014.
- [5] M. Joerger, and B. Pervan, "Kalman Filter-Based Integrity Monitoring Against Sensor Faults," *AIAA Journal of Guidance, Control and Dynamics*, vol. 36, no. 2, pp. 349–361, 2013.
- [6] M. Joerger, and B. Pervan, "Multi-Constellation ARAIM Exploiting Satellite Geometry Change," in *Proc. ION GNSS+*, Tampa, FL, 2015.
- [7] M. Brenner, "Integrated GPS/Inertial Fault Detection Availability," *NAVIGATION, Journal of The Institute of Navigation*, vol. 43, no. 2, pp. 111–130, 1996.
- [8] J. E. Angus, "RAIM with Multiple Faults," *NAVIGATION, Journal of The Institute of Navigation*, vol. 53, no. 4, pp. 249–257, 2006.
- [9] J. Blanch, T. Walter, P. Enge, "Fixed Subset Selection to Reduce Advanced RAIM Complexity," in *Proc. ION ITM*, Reston, VA, 2018.
- [10] R. G. Brown, P. Y. C. Hwang, *Principles of GNSS, inertial, and multisensor integrated navigation systems*, 2nd ed. London, NY: Artech House, 2013.